

Abstract

Alzheimers disease is terrible.

Introduction

Something about AD...

Materials and Methods

Imaging

Cortical thickness

Cross-sectional processing

In [1] we introduced the ANTs cortical thickness processing pipeline using a large cohort of ~ 1200 images taken from four popular, publicly available data sets with ages ranging from 4 to 97 years. The processing pipeline comprises the following four major steps:

- N4 bias correction [2],
- skull stripping [3],
- *n*-tissue segmentation [4], and
- cortical thickness estimation [5]

which is enhanced by the use of optimal shape and intensity templates derived from the specific populations of study. Regional statistics were quantified by parcellating the cortex using a collection of 20 atlases which were labeled using the Desikan-Killiany-Tourville (DKT) protocol [6] consisting of 31 labels per hemisphere (see Table 1). Consensus labelings in each subject were generated from the joint-label fusion approach of [7]. An thickness-based evaluation with the well-known FreeSurfer algorithm demonstrated better predictive performance of age and gender. Since the original publication, we have added the optional inclusion of patch-based denoising based on an ANTs implementation of the patch-based denoising algorithm of [8]. The resulting regional statistics (including cortical thickness, surface area [9], volumes, and Jacobian determinant values) were posted online (<https://github.com/ntustison/KapowskiChronicles>). These include the corresponding FreeSurfer measurements which are also available for public consumption [10]. Since publication, this pipeline has been used in a number of cross-sectional studies [11–13].

Longitudinal processing

The ANTs longitudinal cortical thickness pipeline extends the ANTs cortical thickness pipeline to unbiased longitudinal studies. The pipeline first creates a shape and appearance average subject-specific template (SST) for each individual. It then rigidly aligns each time point to the SST to reduce the effect of coordinate system or interpolation bias. Subsequent processing segments the SST into six probabilistic tissues classes: cerebrospinal fluid (CSF), gray matter (GM), white matter (WM), deep gray matter (striatum + thalamus), brain stem, and cerebellum. This requires processing the SST through two parallel workflows. First, the SST proceeds through the standard ANTs cortical thickness pipeline which generates a brain extraction mask and the CSF posterior probability map. Second, using a data set of expert annotations [6], a class-leading multi-atlas joint label fusion step [7] is performed to create individualized probability maps for all tissue types. This final version of the SST enables unbiased mappings to the group template, subject-specific tissue segmentations, region of interest volumes and cortical thickness maps for each of the original time series images. The corresponding cortical labelings (generated using a multi-atlas label fusion approach and a selected cortical parcellation pro-

Table 1: The 31 cortical labels (per hemisphere) of the Desikan-Killiany-Tourville atlas.

1) caudal anterior cingulate	17) pars orbitalis
2) caudal middle frontal	18) pars triangularis
3) cuneus	19) pericalcarine
4) entorhinal	20) postcentral
5) fusiform	21) posterior cingulate
6) inferior parietal	22) precentral
7) inferior temporal	23) precuneus
8) isthmus cingulate	24) rostral anterior cingulate
9) lateral occipital	25) rostral middle frontal
10) lateral orbitofrontal	26) superior frontal
11) lingual	27) superior parietal
12) medial orbitofrontal	28) superior temporal
13) middle temporal	29) supramarginal
14) parahippocampal	30) transverse temporal
15) paracentral	31) insula
16) pars opercularis	

tocol) are then used to tabulate regional thickness and area values for statistical analysis. Other modalities are then mapped to the group template through these unbiased transformations, as in [14, 15]

Pseudo-geodesic for large cohort labeling.

**Note to self: Add an image and discussion of the pseudo-geodesic for minimizing malf-labeling.
We should also discuss the ants implementation (multi-threading, etc.)**

Statistical methods

We used a simple statistical principle to compare performance between cross-sectional and longitudinal processing methods. We said that one method outperforms the other when it does a better job minimizing within-subject variability and maximizing between-subject variability in cortical thickness measurements. Such a quality implies greater within-subject reproducibility while distinguishing between patient subpopulations. As such this will amount to higher precision when cortical thickness is used as a predictor variable or model covariate in statistical analyses upstream. This criterion is immediately assessable in terms of estimates associated to the longitudinal mixed-effects model outlined below.

As previously noted we observed yearly cortical thickness measurements from sixty-two separate regions of interest. To assess the above variance criterion while accounting for changes that may occur through the passage of time, we used a hierarchical Bayesian model for parameter estimation. Let Y_{ij}^k denote the i^{th} individual's cortical thickness measurement corresponding to the k^{th} region of interest at measurement j . Under the Bayesian paradigm we utilized a model of the form

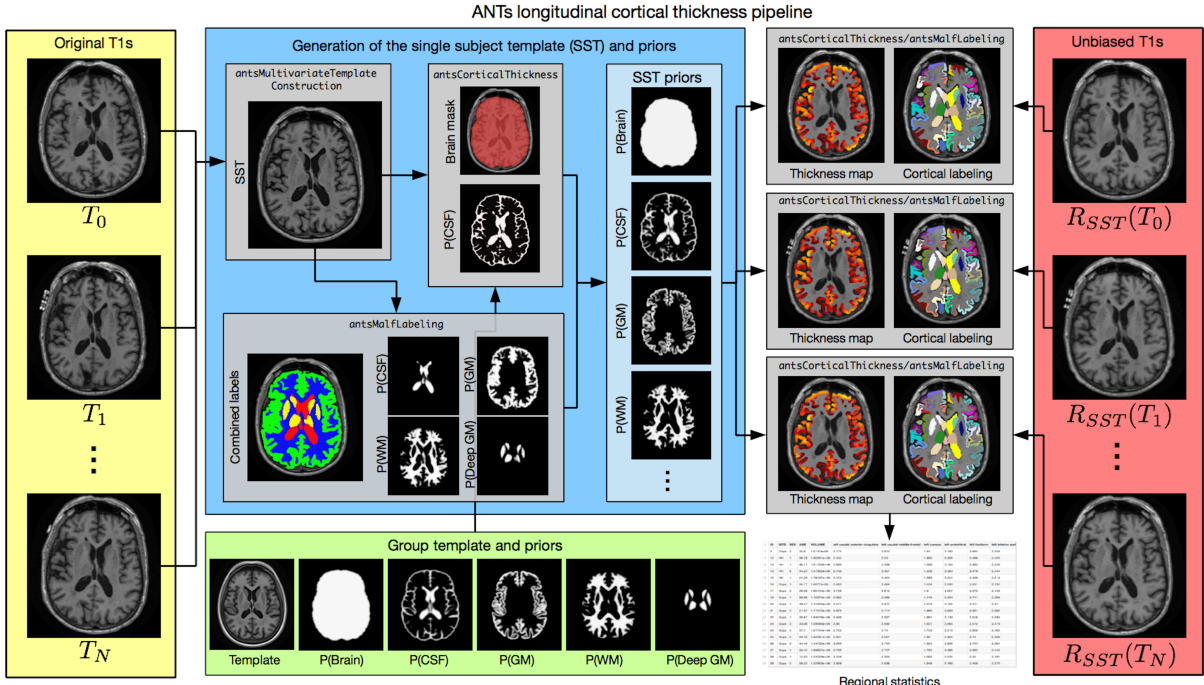


Figure 1: The ANTs longitudinal cortical thickness pipeline. The original T1-weighted images are used to generate an unbiased single-subject template (SST). The SST is then processed via the segmentation portion of the ANTs cross-sectional cortical thickness pipeline reported in [14] using the group template and tissue priors. This results in a probabilistic estimate of the CSF and the brain mask. Joint label fusion (JLF) of 20 atlases involving six labels (CSF, gray matter, white matter, deep gray matter, brain stem, and cerebellum) is used to get a probabilistic estimate of the six tissues. The latter five JLF probabilistic tissue estimates are used as the SST prior probabilities whereas the CSF SST prior probability is derived as a combination of the JLF and segmentation CSF estimates, i.e., $P(CSF) = \max(P_{Seg}(CSF), P_{JLF}(CSF))$. The T1-weighted image at each time point is rigidly aligned to the template and processed through original cortical thickness pipeline using the SST template and auxiliary images (brain extraction mask and tissue priors). Cortical labelings obtained using JLF are then used to quantify ROI-based statistics.

$$\begin{aligned} Y_{ij}^k &\sim N(\alpha_i^k + \beta^k t, \sigma_k^2) \\ \alpha_i^k &\sim N(\alpha_0^k, \tau_k^2) \quad \alpha_0^k, \beta^k \sim N(0, 10) \quad \sigma_k^2, \tau_k^2 \sim \text{Cauchy}^+(0, 5) \end{aligned} \tag{1}$$

Specification of parameters in the above prior distributions reflect commonly accepted diffuse priors. τ_k^2 represents the between-subject variance parameter, and σ_k^2 represents the within-subject variance parameter. For each region, the quantity of interest is thus the ratio $r^k = \frac{\tau_k^2}{\sigma_k^2}$. This ratio is closely related to the intraclass correlation coefficient [16]. The posterior distribution of r^k was summarized via the posterior median. Where the posterior distributions were obtained using Stan probabilistic programming language [17].

For each processing method we performed sixty-two independent regressions. In order to compare results between methods, we considered the quantity $\delta^k = r_l^k - r_c^k$ and $\delta_{norm}^k = \frac{r_l^k - r_c^k}{r_l^k + r_c^k}$, denoting the variance ratio for the longitudinal method minus that of the cross-sectional method and the normed difference between ratios, respectively. Since a large r^k implies a higher between-subject to within-subject variability ratio, a positive estimate of δ^k that is large in magnitude implies that the longitudinal processing method is preferable to the cross-sectional method. Conversely, a negative estimate that is large in magnitude implies that the cross-sectional processing method is preferable to the longitudinal method.

Results

Discussion

Subsection 1

And a sweet equation:

$$\exp^{-i\pi} = -1$$

References

1. Tustison, N. J., Cook, P. A., Klein, A., Song, G., Das, S. R., Duda, J. T., Kandel, B. M., Strien, N. van, Stone, J. R., Gee, J. C., and Avants, B. B. “**Large-Scale Evaluation of ANTs and FreeSurfer Cortical Thickness Measurements**” *Neuroimage* 99, (2014): 166–79. doi:10.1016/j.neuroimage.2014.05.044
2. Tustison, N. J., Avants, B. B., Cook, P. A., Zheng, Y., Egan, A., Yushkevich, P. A., and Gee, J. C. “**N4ITK: Improved N3 Bias Correction**” *IEEE Trans Med Imaging* 29, no. 6 (2010): 1310–20. doi:10.1109/TMI.2010.2046908
3. Avants, B. B., Klein, A., Tustison, N. J., Woo, J., and Gee, J. C. “**Evaluation of an Open-Access, Automated Brain Extraction Method on Multi-Site Multi-Disorder Data**” (2010):
4. Avants, B. B., Tustison, N. J., Wu, J., Cook, P. A., and Gee, J. C. “**An Open Source Multivariate Framework for n-Tissue Segmentation with Evaluation on Public Data**” *Neuroinformatics* 9, no. 4 (2011): 381–400. doi:10.1007/s12021-011-9109-y
5. Das, S. R., Avants, B. B., Grossman, M., and Gee, J. C. “**Registration Based Cortical Thickness Measurement**” *Neuroimage* 45, no. 3 (2009): 867–79. doi:10.1016/j.neuroimage.2008.12.016
6. Klein, A. and Tourville, J. “**101 Labeled Brain Images and a Consistent Human Cortical Labeling Protocol**” *Front Neurosci* 6, (2012): 171. doi:10.3389/fnins.2012.00171
7. Wang, H., Suh, J. W., Das, S. R., Pluta, J. B., Craige, C., and Yushkevich, P. A. “**Multi-Atlas Segmentation with Joint Label Fusion**” *IEEE Trans Pattern Anal Mach Intell* 35, no. 3 (2013): 611–23. doi:10.1109/TPAMI.2012.143
8. Manjón, J. V., Coupé, P., Martí-Bonmatí, L., Collins, D. L., and Robles, M. “**Adaptive Non-Local Means Denoising of MR Images with Spatially Varying Noise Levels**” *J Magn Reson Imaging* 31, no. 1 (2010): 192–203. doi:10.1002/jmri.22003
9. Lehmann, G. and Legland, D. “**Efficient N-Dimensional Surface Estimation Using Crofton Formula and Run-Length Encoding**” *Insight Journal* (2012):
10. Hasan, K. M., Mwangi, B., Cao, B., Keser, Z., Tustison, N. J., Kochunov, P., Frye, R. E., Savatic, M., and Soares, J. “**Entorhinal Cortex Thickness Across the Human Lifespan**” *J Neuroimaging* 26, no. 3 (2016): 278–82. doi:10.1111/jon.12297
11. Price, A. R., Bonner, M. F., Peele, J. E., and Grossman, M. “**Converging Evidence for the Neuroanatomic Basis of Combinatorial Semantics in the Angular Gyrus**” *J Neurosci* 35, no. 7 (2015): 3276–84. doi:10.1523/JNEUROSCI.3446-14.2015
12. Wisse, L. E. M., Butala, N., Das, S. R., Davatzikos, C., Dickerson, B. C., Vaishnavi, S. N., Yushkevich, P. A., Wolk, D. A., and Alzheimer’s Disease Neuroimaging Initiative. “**Suspected Non-AD Pathology in Mild Cognitive Impairment**” *Neurobiol Aging* 36, no. 12 (2015): 3152–62. doi:10.1016/j.neurobiolaging.2015.08.029
13. Betancourt, L. M., Avants, B., Farah, M. J., Brodsky, N. L., Wu, J., Ashtari, M., and Hurt, H. “**Effect of Socioeconomic Status (SES) Disparity on Neural Development in Female African-American Infants at Age 1 Month**” *Dev Sci* (2015): doi:10.1111/desc.12344
14. Tustison, N. J., Avants, B. B., Cook, P. A., Kim, J., Whyte, J., Gee, J. C., and Stone, J. R. “**Logical Circu-**

larity in Voxel-Based Analysis: Normalization Strategy May Induce Statistical Bias” *Hum Brain Mapp* 35, no. 3 (2014): 745–59. doi:10.1002/hbm.22211

15. Avants, B. B., Duda, J. T., Kilroy, E., Krasileva, K., Jann, K., Kandel, B. T., Tustison, N. J., Yan, L., Jog, M., Smith, R., Wang, Y., Dapretto, M., and Wang, D. J. J. “**The Pediatric Template of Brain Perfusion**” *Sci Data* 2, (2015): 150003. doi:10.1038/sdata.2015.3

16. Bartko, J. J. “**On Various Intraclass Correlation Reliability Coefficients.**” *Psychological bulletin* 83, no. 5 (1976): 762.

17. Carpenter, B., Gelman, A., Hoffman, M., Lee, D., Goodrich, B., Betancourt, M., Brubaker, M. A., Guo, J., Li, P., and Riddell, A. “**Stan: A Probabilistic Programming Language**” *J Stat Softw* (2016):